Image-Based Computational Models for TAVI Planning: From CT Images to Implant Deployment

Sasa Grbic[1,2], Tommaso Mansi[1], Razvan Ionasec[1], Ingmar Voigt[1], Helene Houle[4], Matthias John[3], Max Schoebinger[3], Nassir Navab[2], and Dorin Comaniciu[1]

[1] Imaging and Computer Vision, Siemens Corporate Research, Princeton, USA
[2] Computer Aided Medical Procedures, Technical University Munich, Germany
[3] Siemens AG, Healthcare Sector, Forchheim, Germany
[4] Siemens, Healthcare Sector, Mountain View, USA

Abstract. Transcatheter aortic valve implantation (TAVI) is becoming the standard choice of care for non-operable patients suffering from severe aortic valve stenosis. As there is no direct view or access to the affected anatomy, accurate preoperative planning is crucial for a successful outcome. The most important decision during planning is selecting the proper implant type and size. Due to the wide variety in device sizes and types and non-circular annulus shapes, there is often no obvious choice for the specific patient. Most clinicians base their final decision on their previous experience. As a first step towards a more predictive planning, we propose an integrated method to estimate the aortic apparatus from CT images and compute implant deployment. Aortic anatomy, which includes aortic root, leaflets and calcifications, is automatically extracted using robust modeling and machine learning algorithms. Then, the finite element method is employed to calculate the deployment of a TAVI implant inside the patient-specific aortic anatomy. The anatomical model was evaluated on 198 CT images, yielding an accuracy of $1.30 \pm 0.23\, mm$. In eleven subjects, pre- and post-TAVI CT images were available. Errors in predicted implant deployment were of $1.74 \pm 0.40\, mm$ in average and $1.32\ mm$ in the aortic valve annulus region, which is almost three times lower than the average gap of $3\ mm$ between consecutive implant sizes. Our framework may thus constitute a surrogate tool for TAVI planning.

1 Introduction

Valvular heart disease (VHD) affects a large number of people and often requires costly diagnostic, interventional procedures and long-term management [1]. Traditionally, valvular heart disease has been treated with surgical repair or replacement. Over the last years, there have been important advances in concepts, tools, techniques, and patient selection for treatment of valvular heart disease using nonsurgical procedures. One of the most prevalent procedures is the transcatheter valve implantation (TAVI) where a replacement valve is delivered via a catheter using one of several access methods: transfemoral, transapical,

K. Mori et al. (Eds.): MICCAI 2013, Part II, LNCS 8150, pp. 395–402, 2013.

subclavian and direct aortic. The procedure offers the potential to reduce procedural morbidity, mortality, and costs of valve treatment and is currently being utilized in non-operable and high-risk surgical patients [2].

In the current field of medical image analysis there has been several proposals to construct geometric models from established diagnostic modalities. In the context of valvular disease management, the authors in [3] proposed to estimate mitral valve models from MRI. The modeling of the aortic valve from cardiac CT was investigated in [4,5,6]. The models extracted using the previous methods can provide important biomarkers for patient selection and procedure planning such as aortic valve annulus diameters for device sizing. However due to the non-circular annulus shapes, the vast number of device types and sizes, there is often no obvious choice for the specific patient based solely on diameter measurements. Moreover, the effect of the stiff calcifications on implant deployment may be difficult to predict solely based on images. More advanced planning tools are thus required.

At the same time, researchers are developing detailed computational models of valve biomechanics and implant properties to simulate TAVI [7]. In [8], the authors computed TAVI deployment on a patient-specific anatomy calculated from CT image. They obtained promising results with non-linear, hyper-elastic model of aortic apparatus. In [9], the authors investigated the radial force generated by Medtronic - CoreValve and Edwards Sapien device. However, to the best of our knowledge, little validation against postoperative clinical data has been reported so far. Furthermore, current methods rely on tedious manual delineations of the aortic apparatus, which hinders the necessary large scale validation studies.

In this paper, we propose a framework to automatically estimate a patient-specific model of the aortic valve and compute implant deployment. Using robust machine learning techniques, we automatically segment the complete aortic apparatus, including calcifications (Sec. 2). We then employ finite element models of aortic valve to predict the configuration of the implant in the patient-specific anatomy after deployment. The anatomical model was evaluated on 198 3D CT data (Sec. 3). On eleven of them, pre- and post- TAVI images were available. We could therefore quantify the prediction power of our framework in these patients, yielding an accuracy of almost three times lower in average than device sizing gaps. Sec. 4 concludes the paper.

2 Method

Starting from a clinical pre-operative 3D CT image (Fig. 2), we automatically segment the aortic valve model using machine-learning algorithms and generate a patient-specific anatomical model of the aortic valve suitable for simulations (Sec. 2.1). We then apply the biomechanical model of the valve and the CoreValve implant (Sec. 2.2) to compute device deployment for TAVI planning. Finally we compare the computed geometry of the deployed implant with a ground-truth annotation extracted from the post-operative CT.

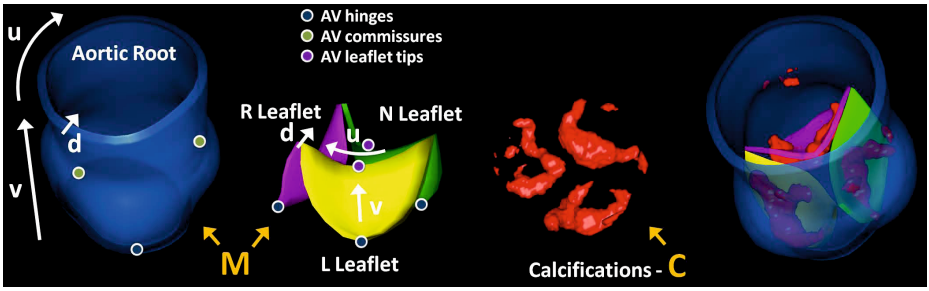

Fig. 1. Diagram showing the estimation framework for the volumetric aortic valve model, which consists of 9 landmarks m (3 commissures, 3 hinges and 3 leaflet tips), aortic root and aortic leaflet volumetric models M, and aortic valve calcifications C

2.1 Parametrization and Estimation of Aortic Valve Morphology

Aortic Model Parameterization. We propose a physiological and volumetric model of the aortic valve capable to capture complex morphological and pathological variations. The anatomical structures consist of nine landmarks including three commissures, three hinges, three leaflet tips, the aortic root, aortic leaflets and calcifications. To efficiently handle the anatomical complexity, the model representation and corresponding parameterization is constructed hierarchically using 1) a non-rigid landmark model m and 2) two volumetric models M and C for the anatomy structure and calcifications respectively (Fig. 1).

The landmarks m define key anatomical structures of the aortic valve and are modeled with nine points: R-, N- and L-hinges, NL-, RN-, NL-commissures, N-, L- and R-leaflet tips. The aortic root and three leaflets are parameterized using a rectangular grid which intrinsically captures volumetric information through a depth parameter d. More precisely, each of the four anatomical structures is spanned across three dimensions, two physiologically aligned curvilinear dimensions u and v, and the third dimension d which defines the thickness in a specific region of the anatomy. For the aortic root, u and v define circumferential and longitudinal directions respectively. For the leaflets, u and v are defined as paraboloids, as illustrated in Fig. 1.

Aortic Valve Detection. Based on the pre-operative CT, herein denoted I, the landmarks m are estimated within the Marginal Space Learning (MSL) framework by maximizing the conditional probability $p(m\,|\,I\,)$, which is based on training and detecting on marginal spaces using the Probabilistic Boosting Tree (PBT) with Haar and steerable features [4]. The vertices of the surface model M are estimated like in [4], where robust machine learning techniques are used to maximize the conditional probability $p(M\,|m, I\,)$. Due to limited image resolution and quality within our data set the volumetric dimension d is fixed to nominal clinical values as reported in [10]. This step could be later replaced by estimating patient specific thickness parameters.

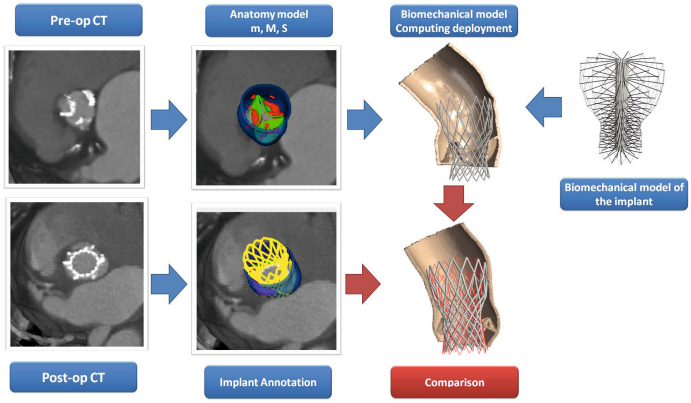

Fig. 2. Diagram showing our validation framework

Calcification Detection. We utilize a discriminative learning approach to segment the calcifications within the aortic valve by maximizing the probability $p(C\,|M, m, I\,)$. We train a boosting classifier and utilize steerable and novel geometric features x_i in order to distinguish the calcified regions within the valve. More precisely, the geometric features x_i are defined as distances to the previously estimated anatomical landmarks m (Fig. 1): $x_i(j = 1 \ldots 9) = ||i - m_j||\,,\ i \in \mathbb{R}^3,\ j = 1, \ldots, 9$. The intuition behind these geometric features is to capture geometric information of tissue distribution relative to the hinge, commissures and leaflet tips landmarks m. Finally, we constrain the spatial search for the classifier with the previously estimated volumetric model M. The system is trained using user-defined thresholds for each training volume.

Implant Parameterization. The CoreValve implant is modeled as a tubular mesh grid aligned along the circumferential u and longitudinal v direction. We utilize a manual annotation framework to fit the ground-truth implant model to the post-operative CT data.

2.2 Finite Element Model of the Aortic Valve and CoreValve

From the segmentation estimated in Sec. 2.1, we build a volumetric, tetrahedral mesh whose elements are automatically tagged according to the structure it belongs to (aortic root, leaflets, calcification). The model is cut at the inflection of the aorta for computational efficiency (Fig. 3). The volumetric mesh is then used to compute the deformation of the aortic apparatus induced by the deploying implant. To that end, we solve the dynamics system $\mathrm{M}\ddot{\mathbf{U}}+\mathrm{C}\dot{\mathbf{U}}+\mathrm{K}\mathbf{U} = \mathbf{F}_c$, where M is the lumped mass matrix, calculated from the mass density of the tissue ($\rho_t = 1070g/L$) and of the implant ($\rho_s = 6450g/L$), K is the stiffness matrix, encoding material properties, C is a Rayleigh damping, whose coefficients for mass and stiffness matrix are both equal to 0.1, $\mathbf{U}$ is the displacement of the nodes of the objects in the scene and $\mathbf{F}_c$ is the vector gathering the external forces resulting from self-collisions and collisions with the implant stent.

Tissue Model. In this work, aortic tissue is modeled with linear isotropic elasticity for computational efficiency, although our framework can easily accommodate for more realistic hyper-elastic constitutive laws that better capture the non-linear behavior of aortic tissues. Poisson ratio ν and Young's moduli E are defined per tissue type: Aortic root: $E = 2\,MPa$, $\nu = 0.48$; Aortic leaflets: $E = 1\,MPa$, $\nu = 0.48$; Calcifications: $E = 60\,GPa$, $\nu = 0.3$ [8]. Co-rotational FEM are employed to cope with large deformations.

CoreValve Model. The CoreValve implant is modeled using a spring model whose stiffness is calculated directly from the specifications of the device (Young's modulus $E = 75\,GPa$). To mimic the shape-memory deployment, the model is deformed according to springs defined between the undeployed and deployed configurations (Fig. 3, right panel). The stiffness of these springs, $k = 1MPa$ (determined off-line), is the minimal stiffness necessary to fully undeploy the implant when free from interactions of any neighboring structures.

Boundary Conditions. The aortic apparatus is tethered to the left ventricle and the aorta. To mimic the compliance of these neighboring organs, aortic annulus and aortic root are tethered in space through springs whose stiffness is equal to $10\,MPa$ (Fig. 3). We ignored the pressure gradients as in the clinical practice rapid pacing is applied before implant deployment. This ameliorates the effect of pressure gradients between the aorta and the left ventricle.

Contacts. Implant / valve contacts and valve self-contacts are modeled using sphere contact models. For instance, for each vertex of the aortic root, a sphere of radius of $1\,mm$ is defined. As soon as a vertex of any object (implant / valve) enters the area defined by this sphere, a spring of stiffness $100\,kPa$ is added between the two vertices to avoid contact. A contact friction of 0.1 is assumed based on [8]. The contribution of the contact forces are gathered into the contact force vector $\mathbf{F}_c$.

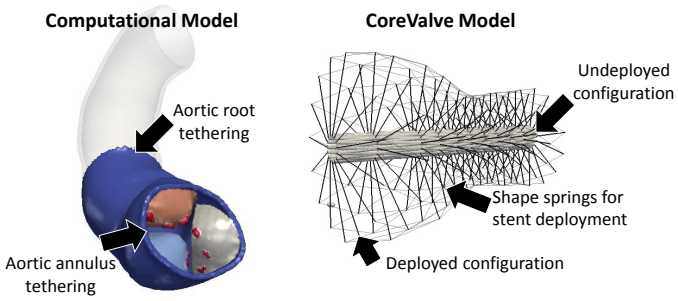

Fig. 3. *Left panel*: anatomical model estimated from the images. Colors encode the different anatomical parts, in red are the calcifications. Arrows indicate spatial tethering. *Right panel*: CoreValve model. Thick black lines represent the strings used to model shape-memory deployment.

Implementation. The model is implemented using the SOFA framework[1]. Spatial discretization is done using linear tetrahedra. An implicit Euler scheme is employed for time integration as it is unconditionally stable.

3 Experimental Results

3.1 Anatomical Model Evaluation

We first evaluated the accuracy of the automatically detected anatomical model M and C on 198 contrasted 3D CT images from stenotic patients with severe calcifications undergoing the TAVI procedure. Three-fold cross-validation against manual delineations yielded a point-to-mesh error of $1.30 \pm 0.23\,mm$ (mean $\pm$ standard deviation; detection speed: $3.1\,s$ per 3D volume, Intel Core2Duo, 2.66GHz quad core, 2GB RAM).

3.2 Evaluation of Implant Deployment Prediction

We then evaluated the complete framework on eleven patients, for whom pre- and post-operative CT images where available. For these patients, the post-operative valve anatomy and CoreValve implant was obtained through an incremental annotation process guided by experts, which included manual placement of anatomical landmarks and delineation of the valve surface and implant struts model. The preoperative anatomy was detected automatically, corrected by experts if needed, and meshed with an average tetrahedral edge-length of $\approx 1.2\,mm$. For all patients, nominal tissue and implant parameters (Sec. 2.2) were employed to evaluate the robustness of the predictions with respect to tissue properties. Simulation time step was $dt = 1\,ms$. The simulation was stopped when the overall system reached equilibrium.

Nine out of eleven cases had the aortic leaflets closed in the preoperative image. In order to be able to place the virtual CoreValve device, we artificially opened the leaflets by applying a pressure of $80\,mmHg$ to their ventricular surface. Tissue and simulation parameters were kept unchanged. Then, once the valve was open, the undeployed CoreValve was placed according to the postoperative anatomy in order to reproduce as close as possible the real intervention. More precisely, the post-to-pre rigid transformation T between the aortic root model $M_{root_{post}}$ and $M_{root_{pre}}$ was estimated using Procrustes alignment. Based on that transformation, the undeployed implant model was mapped to the preoperative data with the same relative position as in the post-op data. The postoperative implant was also registered to the preoperative data for evaluation purposes.

Fig. 4 reports simulation results on four patients. As one can see, despite the nominal tissue parameters and the relative simplicity of the biomechanical model, the predicted deployed implants were in close agreement with the actual postoperative outcome. More quantitatively, the point-to-mesh error between the

[1] `www.sofa-framework.org`

Table 1. Point-to-mesh distance between computed and ground-truth implant deployment configuration. The average error is $1.73 \pm 0.40\,mm$.

Patient	Point-to-Mesh Error	Patient	Point-to-Mesh Error	Patient	Point-to-Mesh Error
01	$1.77 \pm 1.36\,mm$	05	$2.11 \pm 1.57\,mm$	09	$1.00 \pm 0.85\,mm$
02	$1.86 \pm 1.39\,mm$	06	$1.54 \pm 1.08\,mm$	10	$1.76 \pm 1.30\,mm$
03	$2.36 \pm 1.62\,mm$	07	$1.90 \pm 1.26\,mm$	11	$1.21 \pm 0.94\,mm$
04	$1.44 \pm 1.31\,mm$	08	$2.07 \pm 1.69\,mm$		

Table 2. Average diameter error between computed and ground-truth implant model. Precise results were achieved in the annulus region (ring ID 6) where the error is far below the average 3mm gap between consecutive implant sizes.

Ring ID	Diameter Error	Ring ID	Diameter Error
01	$1.86 \pm 1.44\,mm$	06	$1.32 \pm 0.72\,mm$
02	$1.20 \pm 0.80\,mm$	07	$2.77 \pm 1.21\,mm$
03	$1.04 \pm 0.55\,mm$	08	$4.10 \pm 1.96\,mm$
04	$0.80 \pm 0.58\,mm$	09	$2.68 \pm 2.34\,mm$
05	$1.00 \pm 0.84\,mm$	10	$3.60 \pm 2.56\,mm$

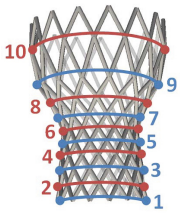

computed deployed implant struts and the ground-truth implant annotation was of $1.73 \pm 0.40\,mm$ (Table 1). In addition we compared implant diameter errors for several key locations along the tubular implant structure (Table 2). As one can see, we could achieve precise results ($1.32\,mm$ error) for the annular ring (ring ID 6), which is the critical area for TAVI intervention. Compared to the usual implant gap of 3mm between implant sizes, our precision has significant accuracy in clinical practice.

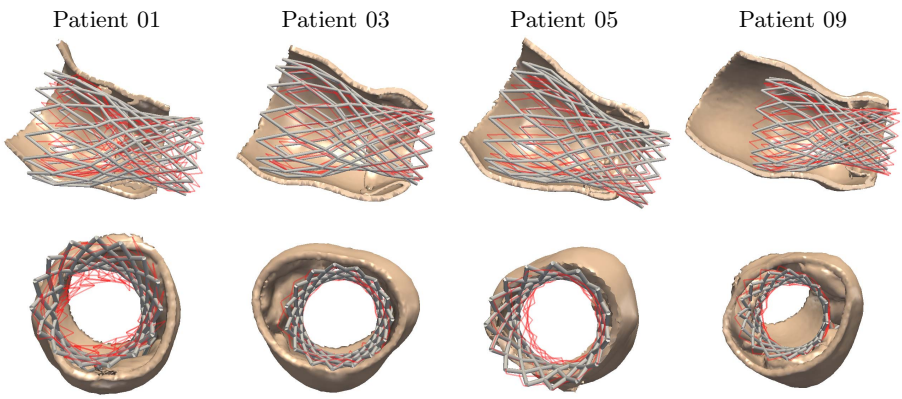

Fig. 4. Example of simulated implant deployment using our automatic volumetric model estimation and our simulation framework. In transparent red is the ground truth. Our model could predict CoreValve deployment based on pre-operative image data only.

4 Conclusion

In this paper we proposed an integrated framework for personalized computation of TAVI deployment. Our approach enables fully automated model extraction from pre-operative CT data and patient-specific implant deployment simulations. We have demonstrated the validity our framework to predict post-operative implant geometry on eleven patients undergoing TAVI with pre- and post-operative data. Regarding the segmentation, future work includes the development of volumetric segmentation algorithms to replace the generic thickness parameters. On the modeling side, anisotropic hyper-elastic materials will be investigated, as well as more accurate models of implant devices. Owing to its automation, our framework may thus constitute a surrogate tool for a more predictive planning of the TAVI procedure.

References

1. John, D., Buellesfeld, L., Yuecel, S., Mueller, R., Latsios, G., Beucher, H., Gerckens, U., Grube, E.: Correlation of Device landing zone calcification and acute procedural success in patients undergoing transcatheter aortic valve implantations with the self-expanding CoreValve prosthesis. JACC. Cardiovascular Interventions 3(2), 233–243 (2010)
2. Kodali, S.K., Williams, M.R., Smith, C.R., Svensson, L.G., Webb, J.G., Makkar, R.R., Fontana, G.P., Dewey, T.M., Thourani, V.H., Pichard, A.D., Fischbein, M., Szeto, W.Y., Lim, S., Greason, P.S., Malaisrie, S.C., Douglas, P.S., Hahn, R.T., Whisenant, D., Akin, J.J., Anderson, W.N., Leon, M.B.: Two-year outcomes after transcatheter or surgical aortic-valve replacement. NEJM 366(18), 1686 (2012)
3. Conti, C.A., Stevanella, M., Maffessanti, F., Trunfio, S., Votta, E., Roghi, A., Parodi, O., Caiani, E.G., Redaell, A.: Mitral valve modelling in ischemic patients: Finite element analysis from cardiac magnetic resonance imaging. In: Computing in Cardiology, pp. 1059–1062 (2010)
4. Ionasec, R.I., Voigt, I., Georgescu, B., Wang, Y., Houle, H., Higuera, F., Navab, N., Comaniciu, D.: Patient-specific modeling and quantification of the aortic and mitral valves from 4-D cardiac CT and TEE. TMI 29(9), 1636–1651 (2010)
5. Waechter, I., Kneser, R., Korosoglou, G., Peters, J., Bakker, N.H., Van Der Boomen, R., Weese, J.: Patient specific models for planning and guidance of minimally invasive aortic valve implantation. In: Jiang, T., Navab, N., Pluim, J.P.W., Viergever, M.A. (eds.) MICCAI 2010, Part I. LNCS, vol. 6361, pp. 526–533. Springer, Heidelberg (2010)
6. Grbic, S., Ionasec, R., Vitanovski, D., Voigt, I., Wang, Y., Georgescu, B., Navab, N., Comaniciu, D.: Complete valvular heart apparatus model from 4D cardiac CT. Medical Image Analysis 16(5), 1003–1014 (2012)
7. Votta, E., Le, T.B., Stevanella, M., Fusini, L., Caiani, E.G., Redaelli, A., Sotiropoulos, F.: Toward patient-specific simulations of cardiac valves: State-of-the-art and future directions. Journal of Biomechanics (2012)
8. Wang, Q., Sirois, E., Sun, W.: Patient-specific modeling of biomechanical interaction in transcatheter aortic valve deployment. Journal of Biomechanics (2012)
9. Tzamtzis, S., Viquerat, J., Yap, J., Mullen, M., Burriesci, G.: Numerical analysis of the radial force produced by the Medtronic-CoreValve and Edwards-SAPIEN after transcatheter aortic valve implantation (TAVI). Med. Eng. & Physics (2012)
10. Freeman, R.V., Otto, C.M.: Spectrum of calcific aortic valve disease: Pathogenesis, disease progression, and treatment strategies. Circulation 111(24), 3316–3326 (2005)